

# The First Compact Objects in the $\Lambda$ -dominated Universe

S. Stachniewicz<sup>1</sup>, M. Kutschera<sup>1,2</sup>

<sup>1</sup>*Astrophysics Division, H.Niewodniczański Institute of Nuclear Physics, ul. Radzikowskiego 152, 31-342 Kraków, Poland*

<sup>2</sup>*Institute of Physics, Jagiellonian University, ul. Reymonta 4, 30-059 Kraków, Poland*

## ABSTRACT

We calculate the evolution of a low-mass ( $M \leq 10^5 M_\odot$ ) spherically symmetric density perturbation in the  $\Omega_b h^2 = 0.02$ ,  $\Omega_M = 0.35$ ,  $\Omega_\Lambda = 0.65$ ,  $h = 0.72$  Universe. The results are compared with the ones that assume no cosmological constant and the flat, dark matter dominated Universe. We include thermal processes and non-equilibrium chemical evolution of the collapsing gas. We find that direct formation of bound objects with such masses by  $z = 8$  is unlikely so in fact they may form only through fragmentation of greater objects. This is in stark contrast to the  $\Omega = 1$  pure CDM cosmology, where low-mass objects form abundantly at redshifts  $z > 10$ .

**Key words:** hydrodynamics – instabilities – dark matter – early Universe.

## 1 INTRODUCTION

Present observations of the CMB anisotropies by the BOOMERANG (Netterfield et al. 2002), MAXIMA-1 (Lee et al. 2001), CBI (Padin et al. 2001) and DASI (Pryke et al. 2002) experiments combined with the data from the Supernova project (Riess et al. (1998); Perlmutter et al. (1999)) suggest that although the geometry of the Universe is flat, its matter content is dominated by the vacuum energy or so-called quintessence. The background cosmology has a very strong influence on the structure formation. In this paper we address the formation of first bound objects in the flat  $\Lambda$ CDM cosmology.

The structure formation on both large and small scales has been studied very carefully in the dark matter dominated cosmology, in particular in the flat pure CDM model. This is not so for the vacuum-energy-dominated models, which are of prime relevance according to the above observations. Perhaps one of the most interesting objects to study are the first bound objects in the Universe – the first quasars and the Population III stars that were the first sources of photons after the light of CMB faded away, and ended the ‘Dark Ages’ of the Universe. Some of these calculations were described in a review by Barkana & Loeb (2001). The recent identification of quasars at  $z \sim 6$  in the Sloan Digital Sky Survey (Fan et al. 2001) strongly motivates such an investigation.

Our code is similar to the one by Thoul & Weinberg (1995) and by Haiman, Thoul & Loeb (1996). We consider the evolution of a single spherically symmetric density perturbation in the early Universe starting soon after recombination until it finally forms a bound stationary object. Our

aim here is to extend their analysis, which was restricted to the  $\Omega = 1$  CDM cosmology, to the  $\Lambda$ -dominated Universe and compare the results with those for the flat, dark matter dominated Universe but with more up-to-date cosmological parameters ( $h = 0.72$ ,  $\Omega_b h^2 = 0.02$ ).

We start tracing the initial expansion of the perturbation at high redshift when its density contrast is still in the linear regime. Then we follow decoupling of the perturbation from the Hubble flow and its subsequent collapse and formation of a virialized cloud. We include the gas dynamics and various cooling and heating processes operating in the expanding and collapsing cloud. The chemical evolution of the collapsing primordial gas cloud is also accounted for.

After the initial collapse, a virialized gas cloud is formed. The kinetic energy of the infalling gas is dissipated through shocks and the cloud becomes pressure-supported. We study the further evolution of the cloud which is determined by its ability to cool sufficiently fast. The most important cooling mechanism for low-mass clouds is the radiation of excited  $H_2$  molecules. The presence of a small amount of the molecular hydrogen  $H_2$  is crucial for triggering the final collapse of such clouds which could form the first luminous object in the Universe.

## 2 NONLINEAR EVOLUTION OF A SPHERICALLY SYMMETRIC DENSITY PERTURBATION

A major approximation we use is the assumption of spherical symmetry. This assumption is best justified in the case of first objects formed in the Universe which are supposed to

originate from the rare highest fluctuations in the primordial density field (Bardeen et al. 1986). It allows us to focus mainly on gas dynamical processes which are expected to control the collapse of low-mass clouds which are supposed to form the first luminous objects.

The spectrum of density fluctuations has more power on small scales, hence the first nonlinear structures are expected to occur on relatively small scales (Miller et al. 1999). As we are interested in small scales, much lower than the horizon, we use Newtonian gravity and treat the expansion of the Universe as a hydrodynamical flow. To describe the evolution of a spherically symmetric density perturbation in the nonlinear regime we use Lagrangian coordinates. We divide both baryonic and dark matter into concentric shells. The dynamics of primordial matter is given by the equations below.

The continuity equation for baryonic matter reads

$$\frac{dM_b}{dr_b} = 4\pi r_b^2 \rho_b, \quad (1)$$

where  $r_b$  is the radius of a sphere of mass  $M_b$ . The radial velocity of the surface of this sphere is

$$\frac{dr_b}{dt} = v_b, \quad (2)$$

and the acceleration satisfies the dynamical equation

$$\frac{dv_b}{dt} = -4\pi r_b^2 \frac{dp}{dM_b} - \frac{GM(r_b)}{r_b^2}, \quad (3)$$

where  $M(r_b) = M_b(r_b) + M_{dm}(r_b) + 2(M_{rad}(r_b) - M_\Lambda(r_b))$  is the total mass within radius  $r_b$  including the effects of radiation and vacuum energy components of the stress-energy tensor. Two last contributions result from the CMB and cosmological constant components of the energy density of the Universe,

$$M_{rad}(r_b) = \frac{H_0^2}{2G} \Omega_{rad}(z+1)^4 r_b^3 \quad (4)$$

and

$$M_\Lambda(r_b) = \frac{H_0^2}{2G} \Omega_\Lambda r_b^3, \quad (5)$$

where  $\Omega_{rad} = 8\pi G a T_{CMB}^4 / (3H_0^2 c^2)$  is the present contribution of the CMB to the total energy density of the Universe in terms of the critical density. Although, as we have shown in (Stachniewicz & Kutschera 2001), at least the radiation component is not negligible, both dark energy and radiation terms are not very important.

The energy conservation condition for baryonic matter reads

$$\frac{du}{dt} = \frac{p}{\rho_b^2} \frac{d\rho_b}{dt} + \frac{\Lambda_{cool}}{\rho_b}, \quad (6)$$

where  $u$  is the internal energy per unit mass,  $p$  is the pressure and  $\rho_b$  is the baryon density. The last term in the eq.(6) describes cooling/heating of the gas, with  $\Lambda_{cool}$  being the energy emission (absorption) rate per unit volume.

We use the equation of state of the ideal gas

$$p = (\gamma - 1)\rho_b u, \quad (7)$$

where  $\gamma = 5/3$ , as the primordial baryonic matter after recombination is assumed to be composed of monoatomic hydrogen and helium with a small (but very important) admixture of molecular hydrogen  $H_2$ .

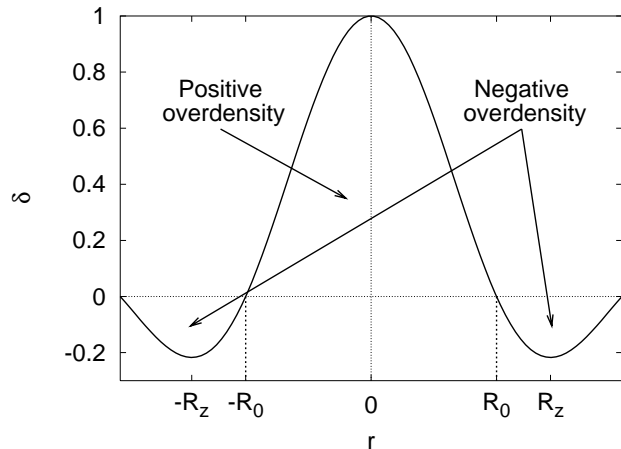


Figure 1. The ‘Sinusoidal’ profile.

Dynamics of dark matter is simpler, as we assume it to be collisionless. The continuity equation is

$$\frac{dM_{dm}}{dr_{dm}} = 4\pi r_{dm}^2 \rho_{dm}, \quad (8)$$

where  $r_{dm}$  is the radius of dark matter sphere of mass  $M_{dm}$ . The radial velocity of this sphere is

$$\frac{dr_{dm}}{dt} = v_{dm}, \quad (9)$$

and the acceleration reads

$$\frac{dv_{dm}}{dt} = -\frac{GM(r_{dm})}{r_{dm}^2}. \quad (10)$$

To solve the above equations we must specify the cooling/heating function  $\Lambda_{cool}$  and the the initial conditions.

### 3 INITIAL CONDITIONS

Let us begin with the initial conditions. We start to follow the evolution of the perturbation soon after the recombination at a sufficiently high redshift that the perturbation is still in the linear regime. We choose the initial redshift to be  $z_i = 500$  like in Haiman et al. (1996).

We apply the initial density profiles in the form of a single spherical Fourier mode used also by Haiman et al. (1996)

$$\rho_i(r) = \Omega_i \rho_c \left(1 + \delta_i \frac{\sin kr}{kr}\right), \quad (11)$$

where  $i = b, dm$  and  $\rho_c$  is the critical density of the Universe,  $\rho_c = 3H^2/8\pi G$  with  $H$  being the actual value of the Hubble parameter. The quantities  $\delta_b$  and  $\delta_{dm}$  measure, respectively, the baryon and dark matter density enhancement with respect to the mean densities  $\bar{\rho}_b = \Omega_b \rho_c$  and  $\bar{\rho}_{dm} = \Omega_{dm} \rho_c$ .

For this profile there exist two distinguished values of the radius,  $R_0$  and  $R_z$  which correspond, respectively, to the first zero and the first minimum of the function  $\sin(kr)/kr$ . They are shown in Fig. 1.

Inside the sphere of radius  $R_0 = \pi/k$  which contains mass  $M_0$ , the local density contrast is positive. The mass  $M_0$  and the radius  $R_0$  will be referred to as the cloud mass

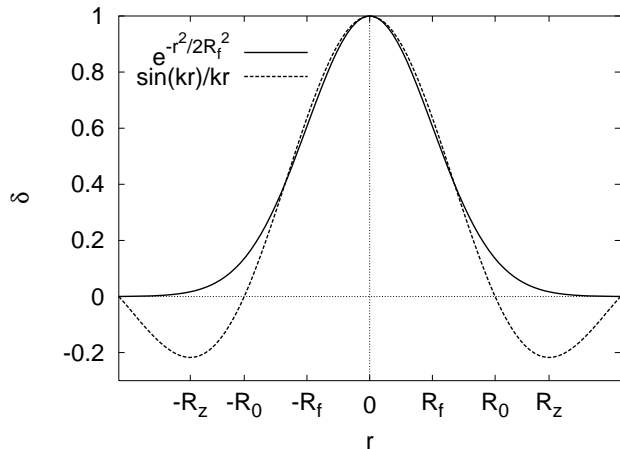


**Figure 2.** Comparison of the ‘Sinusoidal’ profile and the Gaussian one.

and the cloud radius, respectively. The local density contrast is negative for  $R_z > r > R_0$ , with the average density contrast vanishing for the sphere of radius  $R_z = 4.49341/k$  with the mass  $M_z$ . According to the gravitational instability theory in the expanding Universe, the shell of radius  $R_z$  will expand together with the Hubble flow not suffering any additional deceleration. This is why we regard this profile as very convenient in numerical simulations because it eliminates numerical edge effects and mentioned shell simply follows the Hubble expansion of the Universe. It can thus be regarded as the boundary of the perturbation and the mass  $M_z$  will be referred to as the bound mass.

It is worth to note that for radii not greater than  $3/4R_0$  this profile is very similar to the Gaussian profile

$$\varrho_i(r) = \Omega_i \varrho_c \left[ 1 + \delta_i \exp\left(\frac{-r^2}{2R_f^2}\right) \right] \quad (12)$$

with  $R_f = 1/2R_0$ . Both profiles are compared in Fig. 2.

As the initial velocity we use the Hubble velocity for baryon matter,

$$v_b(r) = Hr, \quad (13)$$

whereas for dark matter the initial velocity is (Haiman et al. 1996)

$$v_{dm}(r) = Hr \left( 1 - \frac{1}{3} < \delta_{dm} > r \right). \quad (14)$$

The expression in brackets indicates averaging over the sphere of radius  $r$ . Slower expansion of dark matter at  $z_i = 500$  results from the fact that the dark matter perturbations start to grow earlier than do the baryon matter ones.

Finally, the amplitudes of baryon and dark matter perturbations,  $\delta_b$  and  $\delta_{dm}$  should be specified. To do so one should use the power spectrum corresponding to the initial redshift  $z_i = 500$  that provides rms density fluctuations at a given mass  $M_0$ . For Cold Dark Matter model we use transfer functions calculated using the CMBFAST program by Seljak & Zaldarriaga (1996). The actual value of the rms density fluctuation is equal to

**Table 1.** RMS overdensities for  $\Lambda$ CDM and flat CDM.

$M_0[M_\odot]$	$\sigma_{\Lambda\text{CDM}}$	$\sigma_{\text{CDM}}$
$5 \times 10^2$	0.0539	0.1437
$1 \times 10^3$	0.0518	0.1369
$2 \times 10^3$	0.0496	0.1303
$5 \times 10^3$	0.0469	0.1219
$1 \times 10^4$	0.0449	0.1159
$2 \times 10^4$	0.0429	0.1099
$5 \times 10^4$	0.0404	0.1024
$1 \times 10^5$	0.0385	0.0968

$$\sigma(R, z) = \sqrt{\int_0^\infty \frac{dk}{k} P(k) \tilde{W}(k, R)^2} \quad (15)$$

where  $P(k) = 4\pi d_{norm}^2 100k^n 0.05^{1-n} k^3 t_f(k, z)^2$ . The value of normalization constant  $d_{norm}^2$  may be also obtained from the CMBFAST program.

The rms fluctuation  $\sigma(R, z)$  depends on the shape of the window over which the density is averaged. However, this dependence is quite weak. In the table 1 we list some values for  $z = 500$  obtained by applying this formula to the transfer function and COBE-normalized normalization obtained from CMBFAST to the Gaussian profile of filter radius  $R_f = 1/2R_0$ . Instead of  $R_f$ , we use  $M_0$  which is equal to the total baryonic mass within a sphere of the radius  $R_0$ .

It is worth to note that these results are not much different from the results obtained by applying the fit by Eisenstein & Hu (1999). However, our results are systematically greater by about 23-24% for the  $\Lambda$ -dominated model and by about 7-10% for the pure CDM model. Probably it is due to the fact that the mentioned fit is less accurate for larger redshifts (especially for  $z > 30$ ) and greater  $\Omega_b/\Omega_M$  ratios.

As the baryon density perturbations start to grow only after the recombination, we have decided to set its initial value to  $\delta_{b,i} = 0.1\delta_{dm,i}$  (Haiman et al. 1996). Let us note that CMBFAST predicts  $\delta_{b,i}$  to be about  $0.2\delta_{dm,i}$  in both  $\Lambda$  and dark matter dominated models. However, as we have shown in Stachniewicz & Kutschera (2001), if  $\delta_{b,i}/\delta_{dm,i}$  is 0.2 or less the results are pretty much insensitive to this ratio, runs with its values equal to 0.2, 0.1 and 0.0 were almost indistinguishable.

#### 4 BARYONIC MATTER COMPONENTS, CHEMICAL REACTIONS AND THERMAL EFFECTS

To specify the cooling/heating function  $\Lambda_{cool}$  in Eq.(6) one should include all relevant thermal and chemical processes in the primordial gas. There are many papers discussing the most important contributions to the function  $\Lambda_{cool}$  – see e.g. Katz, Weinberg, Hernquist (1996). All formulas may be found in Stachniewicz & Kutschera (2001).

The primordial gas consists of neutral atoms and

molecules, ions and free electrons. In this paper we have taken into account nine species: H, H<sup>-</sup>, H<sup>+</sup>, He, He<sup>+</sup>, He<sup>++</sup>, H<sub>2</sub>, H<sub>2</sub><sup>+</sup> and e<sup>-</sup>. Some authors (e.g. Galli & Palla (1998)) include also deuterium and lithium.

The abundance of various species can, generally, change with time as the chemical reactions between species occur and the ionization and dissociation photoprocesses take place in the hot gas. The chemical reactions include such processes as e.g. the ionization of hydrogen and helium by electrons, the recombination of ions with electrons, the formation of negative hydrogen ions, the formation of H<sub>2</sub> molecules, etc. The full list of relevant chemical reactions is given in Stachniewicz & Kutschera (2001). Photoprocesses include ionization of neutral hydrogen H, helium He and He<sup>+</sup> by photons, and dissociation of negative hydrogen ions H<sup>-</sup> and H<sub>2</sub> molecules by photons.

Time evolution of the number density of the component  $n_i$  is described by the kinetic equation:

$$\frac{dn_i}{dt} = \sum_{l=1}^9 \sum_{m=1}^9 a_{lmi} k_{lm} n_l n_m + \sum_{j=1}^9 b_{ji} \kappa_j n_j. \quad (16)$$

The first component on the right-hand side of this equation describes the chemical reactions and the other one describes photoionization and photodissociation processes. The coefficients  $k_{lm}$  are reaction rates, the quantities  $\kappa_n$  are photoionization or photodissociation rates and  $a_{lmi}$  and  $b_{ji}$  are numbers equal to 0,  $\pm 1$  or  $\pm 2$  depending on the reaction. All the reaction rates, photoionization and photodissociation rates are given in Stachniewicz & Kutschera (2001).

The cooling (heating) function  $\Lambda_{cool}$  includes emissivities (absorption rates) due to such processes as the collisional ionization of H, He and He<sup>+</sup>, recombination to H, He and He<sup>+</sup>, the collisional excitation of H and He<sup>+</sup>, Bremsstrahlung, the Compton cooling and the cooling by deexcitation of H<sub>2</sub> molecules. The formulae for the heating/cooling contributions of various processes are given in Stachniewicz & Kutschera (2001).

## 5 NUMERICAL CODE AND INITIAL CONDITIONS

The dynamical equations (1)-(10) are solved numerically. At each timestep also the chemical composition of the gas is updated by solving Eq.(16) and the appropriate value of the cooling function  $\Lambda_{cool}$  is calculated. We based our numerical code on the code described by Thoul & Weinberg (1995), which is the standard, second-order accurate, Lagrangian finite-difference scheme. Details of the code are described in Stachniewicz & Kutschera (2001).

We handle timesteps and central boundary conditions in the way proposed by Thoul and Weinberg Thoul & Weinberg (1995). For dark matter, we treat the center as a hard sphere of some "small" radius  $r_c$ . In order not to affect the results of calculations the value of  $r_c$  should be much less than any other characteristic radius in the problem but it should not be too small because smaller  $r_c$  means worse energy conservation and longer computation time. We have chosen  $r_c$  equal to the initial radius of the most innermost dark matter shell. For the baryonic component, if a shell falls

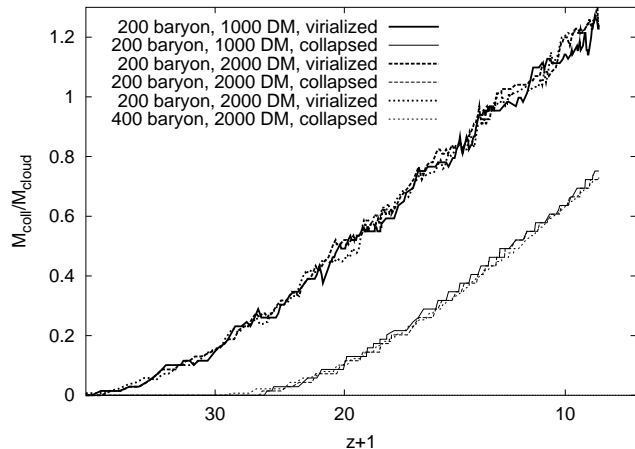


**Figure 3.** Test of accuracy – comparison of runs with various number of baryonic and dark matter shells

below  $r_c$  we assume that it has ‘collapsed’ and fix its radius, temperature and chemical composition.

In the collapse of baryon matter one encounters the formation of shocks. In our code shocks are treated with the artificial viscosity technique (Richtmyer & Morton 1967).

It is worth to mention that set of equations 16 is very stiff and may require very small timesteps. To deal with this problem we follow Haiman et al. (1996) and we used the STIFBS routine from Press et al. (1996).

We have performed two sets of calculations, for the  $\Lambda$ -dominated Universe ( $\Omega_b h^2 = 0.02$ ,  $\Omega_M = 0.35$ ,  $\Omega_\Lambda = 0.65$ ) and for the pure CDM model ( $\Omega_b h^2 = 0.02$ ,  $\Omega_M = 1.0$ ), with  $h = 0.72$  in both cases. We started our calculations at  $z = 500$ . The initial gas temperature and chemical composition were obtained by running our own program that starts at  $z = 10000$  with equilibrium values and ends at a required redshift. We have compared its predictions to the results of Galli & Palla (1998) and the differences were not greater than 10%. One should note that these authors have included more species (e.g. deuterium and lithium) and some of their reaction rates were slightly different. The difference between the temperatures of the baryonic gas and the CBR turned out to be lower than 1% at  $z = 500$ .

For the  $\Lambda$ -dominated model we have performed runs with cloud masses  $M_0$  from 200 to  $10^5 M_\odot$ , for the pure CDM model cloud masses were between 500 and  $5000 M_\odot$ . For each cloud mass we have chosen a few values of the initial dark matter overdensity between 0.07 and 0.40, depending on the mass.

We have divided the baryonic component to 200 concentric shells of equal mass, the dark matter component was divided to 1000 equal mass shells. It turned out to be enough – in Fig. 3 we compare the calculated amount of virialized and collapsed mass for the same initial conditions and three different runs: with 200 baryonic and 1000 dark matter shells, 200 baryonic and 2000 dark matter shells and, finally, with 400 baryonic and 2000 dark matter shells. The results are the same within our numerical accuracy.

## 6 RESULTS

We expect that there will be a significant difference between the low-mass structure formation in the  $\Lambda$ CDM and the Standard CDM models. The main reason is that the rms fluctuations in the dark energy dominated model are about 2.5-2.7 times lower than in the Standard CDM model (table 1). The other one is that in the Standard CDM the average matter density is equal to the critical density so any overdensity would eventually stop its expansion and collapse. In the  $\Lambda$ CDM the matter density is lower, so there is some threshold overdensity necessary for recollapse. Any given overdensity would collapse slower (if at all) than in Standard CDM. It means that in the  $\Lambda$ -dominated Universe there would be much less luminous objects at large redshifts and the first ones would appear much later as compared to the dark matter dominated Universe. In addition, we may expect that the masses of the first collapsed objects would be greater.

The behaviour of dark matter shells plays the crucial role in the cloud collapse as there is much more dark matter than the baryonic matter. By assumption, dark matter is collisionless, so there is no energy loss mechanism apart from possible gravitational energy exchange. The evolution of the dark matter shells in the absence of baryonic matter is that their radii increase to some maximal value, then the shells collapse and after some oscillations due to bounces off the artificial hard sphere the dark matter cloud becomes stationary. In the presence of baryonic matter the behaviour of dark matter shells is similar because the amount of baryonic matter is much lower than the amount of dark matter. The difference is that the average radius of a dark matter shell slowly decreases.

The behaviour of baryon matter shells is that after reaching maximum radii, the shells collapse and the shock develops at some stage due to pressure crowding of neighbouring shells (Haiman et al. 1996). The shock stops the collapse and the baryon shells virialize. Then if the clouds have a sufficient temperature and density for efficient cooling, they can undergo the final collapse.

We assume that the shell has ‘virialized’ if the mean density inside the shell exceeds  $18\pi^2$  times the actual mean baryon density of the Universe. This value was calculated for the top-hat overdensities in the Einstein-de Sitter model but, however, Bryan & Norman (1998) have shown that in the  $\Lambda$ CDM models the dependence on  $\Omega_M$  is not very strong. Of course, this criterion depends on the redshift. For a virialized baryonic shell its radius and density are roughly constant but the mean matter density of the Universe decreases so the overdensity increases. This means that overdensity is not a good criterion of the collapse – we need to take something related to the actual size of the object. We have decided to assume that a shell has ‘collapsed’ if its radius falls below some ‘small’ value, in our case: the initial radius of the cloud  $R_0$ .

The results of our calculations are displayed in Figs. 4 – 8. Perhaps the most interesting are plots that show the evolution of the amount of the collapsed baryonic mass for various cloud masses and initial overdensities. Figs. 4 a-d show the fraction of the cloud mass that meets the collapse criterion at a given redshift for the  $\Lambda$ -dominated Universe. Similar plots for the dark matter dominated Universe are shown in Figs. 5 a-d.

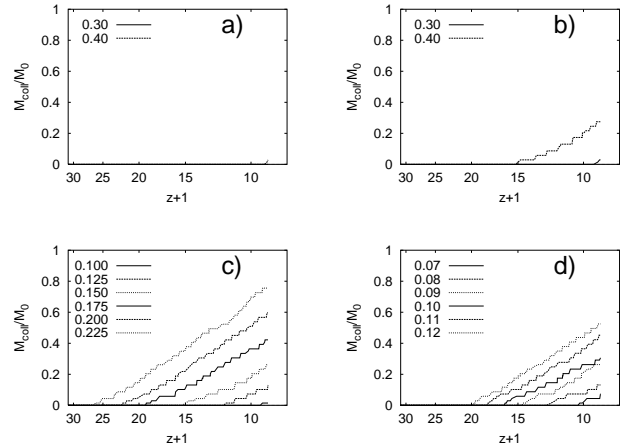


**Figure 4.** The collapsed mass fraction as a function of redshift for  $M_0 = 2 \times 10^3 M_\odot$ ,  $3 \times 10^3 M_\odot$ ,  $2 \times 10^4 M_\odot$  and  $1 \times 10^5 M_\odot$  in the  $\Lambda$ -dominated Universe. Indicated are overdensities corresponding to different curves.

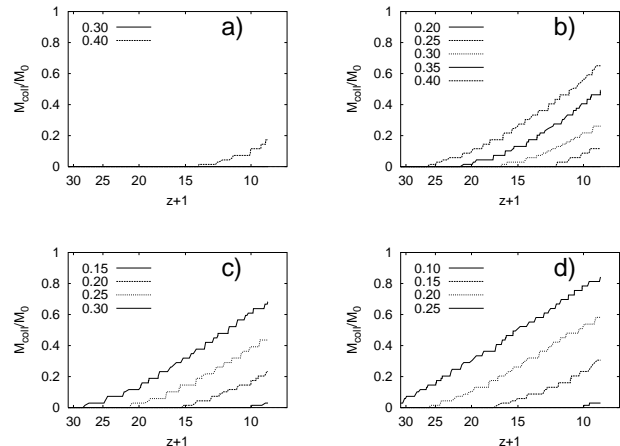


**Figure 5.** The same as in Fig. 4 for  $M_0 = 5 \times 10^2 M_\odot$ ,  $1 \times 10^3 M_\odot$ ,  $2 \times 10^3 M_\odot$  and  $5 \times 10^3 M_\odot$  in the CDM-dominated Universe.

If there is a line that is described but cannot be found on a plot it means that for this overdensity no baryonic shell has collapsed before  $z = 8$ .

The results confirmed our expectations. In the dark energy dominated Universe initial clouds need greater mass and larger initial overdensities in order to at least partially collapse before  $z = 8$ . If we restrict ourselves to clouds of  $z = 500$  DM overdensities not greater than 0.4, the minimal mass needed for at least partial collapse before  $z = 8$  is  $3000 M_\odot$  (Fig. 4 b). For  $M = 2000 M_\odot$  and  $\delta_{dm,i} = 0.4$  the fraction of the collapsed mass is on order two percent (Fig. 4 a). One should remember that for these cloud masses the rms fluctuations at  $z = 500$  are about 0.05 so overdensities equal to 0.4 represent  $8\sigma$  peaks, which are **extremely unlikely**. For the dark matter dominated Universe, the minimal cloud mass is about  $500 M_\odot$  (Fig. 5 a) – for the initial overdensity equal to 0.4 (the rms overdensity is about 0.14) about 9% of the cloud mass may collapse before  $z = 8$ .

If we look at higher masses, the collapse becomes easier and easier, threshold initial overdensities for partial collapse before  $z = 8$  fall much faster than the rms overdensities.

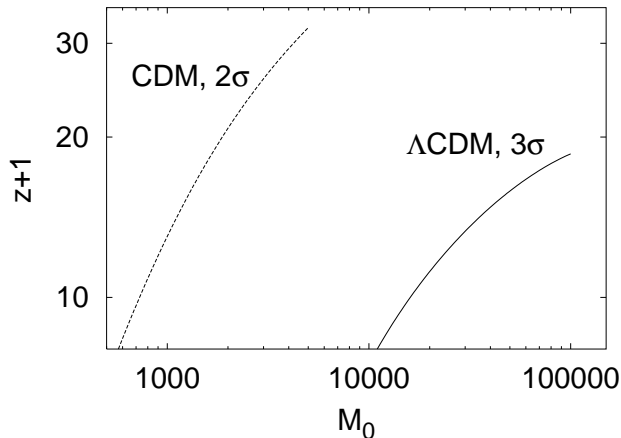


**Figure 6.** Approximate redshift when the object starts its collapse.

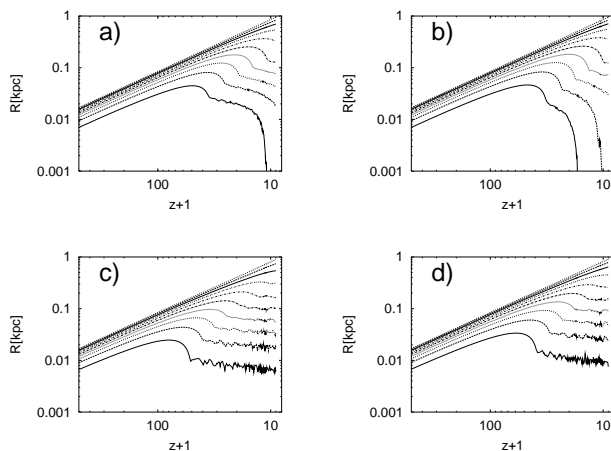


**Figure 7.** Evolution of the baryonic (upper plots) and dark matter (bottom plots) shells for  $M_0 = 5 \times 10^3 M_\odot$ ,  $\delta_{dm,i} = 0.30$  for the  $\Lambda$ -dominated Universe (left) and for  $M_0 = 5 \times 10^3 M_\odot$ ,  $\delta_{dm,i} = 0.20$  for the CDM-dominated Universe (right).

However, for the  $\Lambda$ -dominated Universe and cloud masses not greater than  $10^4 M_\odot$  the clouds need overdensities larger than  $3\sigma$  in order to at least partially collapse – unlike in the flat CDM model. For greater baryonic masses the collapse is a bit more likely but even for  $10^5 M_\odot$  (Fig. 4 d) they need at least  $2\sigma$  to start their collapse before  $z = 8$ .

Fig. 6 shows approximately the redshift when the most innermost shell has collapsed for various masses and  $3\sigma$  overdensities in the  $\Lambda$ CDM Universe and for  $2\sigma$  overdensities in the flat CDM Universe.

In Figs. 7 a-d we compare the evolution of dark matter shells and baryon matter shells of the cloud with mass  $M_0 = 5000 M_\odot$ , for the dark energy and dark matter dominated Universes. The values of initial dark matter density enhancements are, respectively,  $\delta_{dm,i} = 0.30$  and  $\delta_{dm,i} = 0.20$ .

The shells shown on the plots enclose 7%, 17%, 27%, ..., 97% of the bound mass. This fractional division of mass applies to both dark matter and baryon

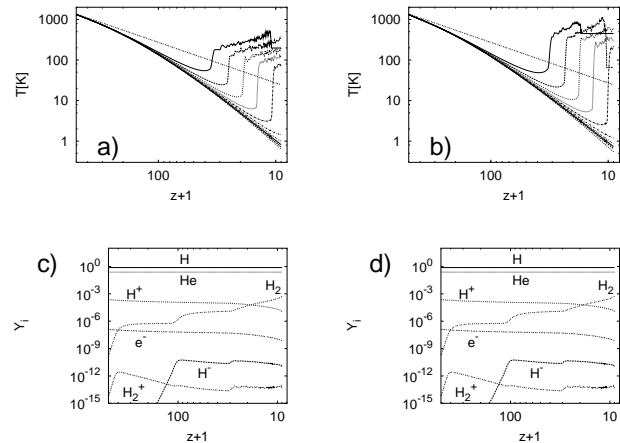


**Figure 8.** Evolution of the shell temperatures and chemical evolution for a shell enclosing 12% of the bound mass, for  $M_0 = 5 \times 10^3 M_\odot$ ,  $\delta_{dm,i} = 0.30$  for the  $\Lambda$ -dominated Universe (left) and for  $M_0 = 5 \times 10^3 M_\odot$ ,  $\delta_{dm,i} = 0.20$  for the CDM-dominated Universe (right).

matter shells. It applies also to the Fig. 8 (plots a and b) that show thermal evolution of gas shells.

The behaviour of both baryonic and dark components is quite typical, very similar to the results of Haiman et al. (1996) and our previous work (Stachniewicz & Kutschera 2001). Dark matter shells expand to some maximum radius, then recollapse to about a half of this value and then very slowly contract. In our calculations the behaviour of dark matter is quite independent of the cloud mass – however, the position and the value of the maximal radius depend on the initial overdensity. In contrast, the behaviour of baryon matter shells strongly depends on the cloud mass and initial overdensity. Of course, higher masses and overdensities cause faster and more violent final collapse.

In Figs. 8 a and b we show the temperature of shells as a function of redshift. The curves indicating temperatures of baryonic shells behave in an opposite way than the radii of baryonic shells. The temperature falls during expansion and increases in the collapse phase. After virialization the temperature remains roughly constant until it starts to fall quite rapidly during the final collapse. These figures show that virial temperatures in Standard CDM are higher than in  $\Lambda$ CDM for objects of the same mass: even though for the  $\Lambda$ CDM cloud initial overdensity was higher (0.3 compared with 0.2), virial temperatures of its shells were about two times smaller. We also have noticed that in both cosmological models shells that undergo the final collapse must reach some critical temperature. For  $\Lambda$ CDM it is about 500 K while for Standard CDM it is about 450 K and it is quite independent on the mass of the cloud. Shells at lower temperatures do not collapse before  $z = 8$ .

The abundance (by mass) of various species as a function of redshift is shown in Figs. 8 c and d. The results correspond to the shell of mass  $M = 0.12 M_z$  of the same cloud as in Figs. 7 and 8 a, b. One can notice the increase of the amount of  $H_2$  molecules at later redshift when the shell collapses. This makes  $H_2$  cooling more efficient, triggering the final collapse of inner shells.

In Figs. 9 a-f we show plots similar to Fig. 7 but normal-

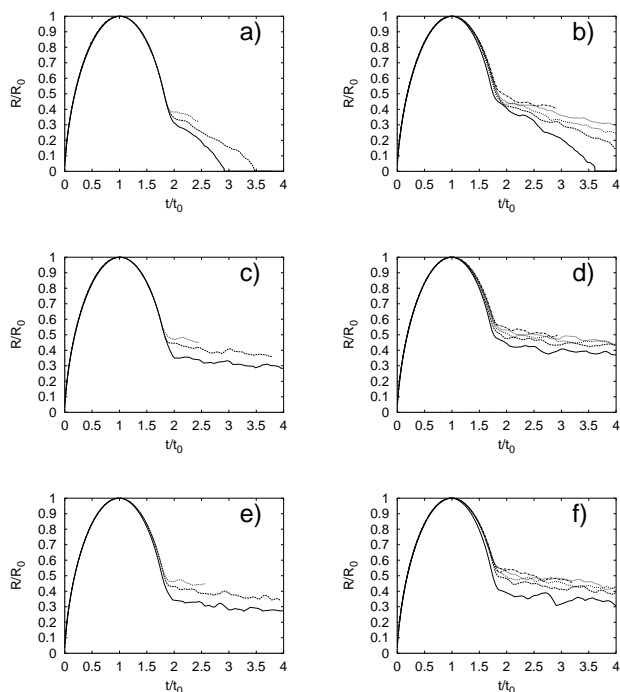


**Figure 9.** Normalized evolution of baryonic shells for  $M_0 = 5 \times 10^3 M_\odot$ ,  $\delta_{dm,i} = 0.30$  for the  $\Lambda$ -dominated Universe (left) and for  $M_0 = 5 \times 10^3 M_\odot$ ,  $\delta_{dm,i} = 0.25$  for the CDM-dominated Universe (right) with cooling (upper plots), without  $H_2$  cooling (plots in the middle) and without any cooling or heating (bottom plots).

ized to the maximum radius  $R_0$  and time of the turnaround  $t_0$  for  $M_0 = 5 \times 10^3 M_\odot$ ,  $\delta_{dm,i} = 0.30$  for the  $\Lambda$ -dominated Universe (plots a, c and e) and for  $M_0 = 5 \times 10^3 M_\odot$ ,  $\delta_{dm,i} = 0.25$  for the CDM-dominated Universe (plots b, d and f) with cooling, without  $H_2$  cooling and without any cooling or heating (including photoionization). While plots with no cooling/heating (e and f) and no  $H_2$  cooling (c and d) are almost self-similar for different shells (the difference in final radii is probably due to different mean initial overdensity for each shell) and similar to those predicted by Bertschinger (Bertschinger 1985), plots with cooling are self-similar and Bertschinger-like up to virialization only. It also shows that  $H_2$  cooling is necessary to collapse before  $z = 8$ .

## 7 CONCLUSIONS

For the dark energy dominated Universe we need very large overdensities, usually much exceeding the  $3\sigma$  limit, for low-mass ( $M_0 \leq 10^5 M_\odot$ ) objects in order to at least partially collapse before  $z = 8$ . For the flat, dark matter dominated Universe the collapse is much faster and direct formation of a low-mass object is quite likely, even as soon as for  $z \sim 20 - 30$ . It is a result of much lower normalization in  $\Lambda$ CDM (Table 1) and lower virial temperatures for  $\Lambda$ CDM clouds of the same mass and initial overdensity. A secondary reason may be that in the flat CDM model any overdensity will stop its evolution and possibly cool and collapse while for  $\Omega_M < 1$  there is some threshold overdensity that depends on the model and epoch. The chemical evolution is pretty much insensitive to cosmology, at least before the fi-

nal collapse. In the  $\Lambda$ -dominated Universe perhaps low-mass objects may form through fragmentation of greater objects. Direct formation of such objects before  $z \sim 10$  seems unlikely.

## REFERENCES

- Bardeen J.M. et al., 1986, ApJ 304, 15  
 Barkana R., Loeb, A., 2001, ARA&A 39, 19  
 Bertschinger E., 1985, ApJS, 58, 39  
 Bryan G.L., Norman M., 1998, ApJ, 495, 80  
 Eisenstein D.J., Hu W., 1999, ApJ 511, 5  
 Fan X. et al., 2001, AJ 122, 2833  
 Galli D., Palla F., 1998, A&A, 335, 403  
 Haiman Z., Thoul A.A., Loeb A., 1996, ApJ 464, 523  
 Katz N., Weinberg D.H., Hernquist L., 1996, ApJS, 105, 19  
 Lee A.T. et al., 2001, ApJ 561, L1  
 Miller A.D. et al., 1999, A&AS 195, 5508  
 Netterfield C.B. et al., 2002, ApJ 571, 604  
 Padin S. et al., 2001, ApJ 549, L1  
 Perlmutter S. et al., 1999, ApJ 517, 565  
 Press W.H., Teukolsky S.A., Vetterling, W.T. Flannery B.P., 1996, Numerical Recipes in C. The Art of Scientific Computing. Second Edition. Cambridge University Press (1996)  
 Pryke C. et al., 2002, ApJ 568, 46  
 Richtmyer R., Morton K.W., 1967, Difference methods for Initial-Value Problems, Interscience Publishers, New York  
 Riess A.G. et al., 1998, AJ 116, 1009  
 Seljak U., Zaldarriaga M., 1996, ApJ 469, 437  
 Stachniewicz S., Kutschera M., 2001, Acta Phys. Pol. B 32, 227  
 Thoul A.A., Weinberg D.H., 1995, ApJ 442, 480